Journal of Ship Research, Vol. 38, No. 4, Dec. 1994, pp. 259–271

Out-of-Plane Solutions and Bifurcations of Submersibles in Free Positive Buoyancy Ascent

Fotis A. Papoulias[1] and **Ibrahim Aydin**[2]

The problem of motion stability of submersible vehicles in free positive buoyancy ascent is analyzed. Motion is allowed to occur in combined vertical and horizontal planes. Continuation and catastrophe theory techniques are employed to trace all possible steady-state solutions in six degrees of freedom, while local linearization reveals their stability properties. Vehicle geometric properties and control surface deflections are used as the primary bifurcation parameters. It is shown that multiple solutions may exist in the form of pitchfork bifurcation, solution separation, hysteresis, and teardrop branches. Regions in parameter spaces are identified where extreme sensitivity of solutions to geometric properties and hydrodynamic modeling is present.

Introduction

THE DYNAMIC response of a submarine under casualty conditions constitutes a crucial, and frequently limiting, factor in establishing the vehicle's submerged operating envelope. As basic casualty conditions in the context of this work, we mean the loss of control surface and/or propulsion system response, or a flooding casualty where the boat must either be brought to the surface or stabilized to a new operating depth. Of particular significance is the study of the ability of the boat to recover from a control surface jam. There exist several factors which determine the severity of such a situation as well as the recovery procedures: the initial conditions (speed, depth, pitch angle, etc.) during the jam, the actual control surface angles, reversing time and backing power of the propulsion system, the ability to blow ballast, and the time between recognition of casualty and initiation of proper recovery procedures. In such a scenario, closed-loop control is kept at a minimal level, and open-loop dynamics become the primary source of evaluation of response qualities. To this end, it is crucial that we have a clear understanding of the dynamics of the boat during a loss of propulsion situation.

A similar need arises in the case of free buoyancy ascent or descent of an autonomous underwater vehicle. Such operations arise frequently in order to dive or rise to the commanded depth while conserving power. The excess buoyancy or weight is the primary means for propulsion in this case and a limited control may be used in the form of predetermined control surface deflections and/or ballast control. Such flight paths are executed under minimal power and, in most cases, in the absence of computer closed-loop control, in order to conserve power. The only means of control authority that we can have in our disposal are predictive capabilities for the vehicle open-loop dynamics.

The traditional methods for establishing dynamic stability of motion concentrate mainly on eigenvalue analysis during small perturbations around nominal straight-line paths (Clayton & Bishop 1982). Two indices are utilized, a stability index G_v for the vertical plane and G_h for the horizontal plane (Roddy 1990). In terms of the slow-motion derivatives, these indices are given by

$$G_v = 1 - \frac{M_w(Z_q + m)}{Z_w(M_q - x_G m)}$$

$$G_h = 1 - \frac{N_v(Y_r - m)}{Y_v(N_r - x_G m)}$$

Positive values for these indices, whose usage dates back to the 1950's, indicate motion stability in the corresponding plane. The above two indices are very useful in design and evaluation of response qualities under most ordinary maneuvering scenarios. The underlying assumption in these criteria is that during normal straight-line motions, the coupling between horizontal and vertical plane motions is relatively weak, and can be neglected. Although vortex shedding and flow separation introduces a certain degree of coupling, the above assumption has been proven quite useful in design and analysis. However, for a high-speed fast-maneuvering submarine operating at the extremes of her submerged operating envelope, or during an emergency situation, the above assumption of uncoupled motions breaks down. High-amplitude motions may take place in all six degrees of freedom, and the nonlinear interactions between the various modes of motion become more pronounced. Therefore, use of the simple G_v, G_h indices may lead to incorrect conclusions, and we have to carefully consider the motion characteristics allowing for coupling between horizontal and vertical planes.

The implications of nonlinear effects and coupling are numerous. In the case of roll motion, which is one of the most critical responses, there is growing evidence of complicated dynamics and chaotic response under certain excitations (Falzarano et al 1992, Falzarano & Zhang 1993, Thompson et al 1991, Virgin & Bishop 1988). In the case of submarine motions, there is evidence of bifurcation phenomena and extreme sensitivity of response to initial conditions and control actions during emergency ascent scenarios such as recovery from a dive plane jam. As motivation for the analysis that follows we present in Fig. 1 typical simulation results using a constant coefficient nonlinear maneuvering model. The time simulation is in terms of vehicle roll angle ϕ versus time for 2% excess buoyancy with the buoyancy force located 1% of the vehicle length forward of the center of gravity, −6 deg

[1]Associate professor, Naval Postgraduate School, Department of Mechanical Engineering Monterey, California.

[2]Lieutenant, Turkish Navy; formerly, Naval Postgraduate School, Department of Mechanical Engineering, Monterey, California.

Revised manuscript received at SNAME headquarters January 20, 1994.

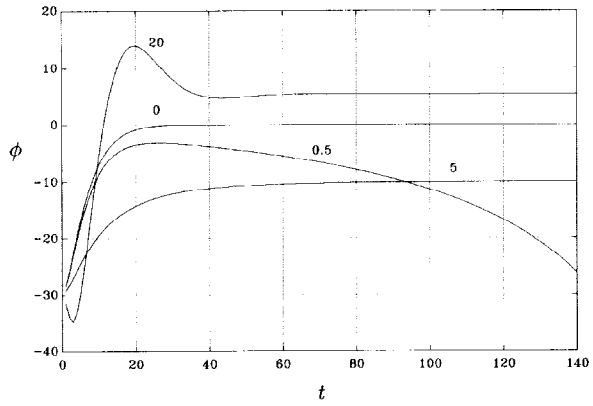

Fig. 1 Time history (ϕ,t) for δ_B = 2%W, x_{GB} = −1%L, δ_s = −5 deg, z_{GB} = 0.1 ft, and for different values of rudder angle

dive plane angle, and 0.1 ft (0.03 m) metacentric height. Four different recovery actions are shown, all parametrized by the applied rudder angle in degrees. It can be seen that although zero rudder angle appears to bring the vehicle roll angle back to zero in the shortest time, the response does not persist. Small nonzero values for the rudder angle develop excessive roll angles in a divergent way, while larger rudder angles reduce the amount of roll. Clearly the vehicle effective rudder angle is largely affected by the amount of vorticity and currents in the flow field, and its actual value cannot be known exactly. Since situations like the one presented in the graph should be avoided, we need to develop a mechanism for assessing those regions in the parameter space where the response cannot be simulated with confidence.

Stability in unpowered ascent has been studied mainly in the vertical plane. In Booth (1977) the vehicle response was distinguished into either a nearly vertical ascent or a predominantly forward motion. In Papoulias & McKinley (1994) it was found that the above distinction is not always meaningful as a result of the many parameters that affect the problem; that is, it was established that the actual motion is a combination of nearly vertical ascents and predominantly forward motions. This latter study maintained some vertical plane restrictions, although it indicated the potential existence of pitchfork bifurcations which led to coupled out-of-plane solutions. In this work we relax the requirement for vertical plane motions and we analyze the stability properties of all possible steady states in six degrees of freedom. This is motivated by both numerical observations (Papoulias & McKinley 1994) and experimental results (Booth 1977), where six-degrees-of-freedom motions were reported. We maintain the assumption of unpowered ascent where the only motion driving mechanism is the amount of excess buoyancy. We employ a combination of singularity theory (Golubitsky & Schaeffer 1985), bifurcation theory (Guckenheimer & Holmes 1983), and numerical continuation (Seydel 1988) methods in order to capture all steady-state solutions that are physically admitted by the coupled nonlinear equations of motion. The primary bifurcation parameters used are: amount and location of excess buoyancy, dive plane and rudder deflection, and the metacentric height. Solution branching is shown to occur in various forms, including single and multiply connected pitchfork bifurcations, separation of solutions, hysteresis, and teardrop branches. We summarize our results in the form of bifurcation graphs which identify parameter regions with qualitatively different asymptotic response characteristics.

For demonstration purposes, all computations in the present work are performed for the Swimmer Delivery Vehicle (SDV), a 17.4 ft (5.3 m) vehicle for which a complete set of hydrodynamic and geometric properties is available (Smith et al 1978). Unless otherwise specified, all results herein are presented in dimensional form, linear dimensions in feet, velocities in feet per second, angular deflections in degrees, and time in seconds.

Problem formulation

Here, we present the equations of motion for the model used in this work. A detailed analysis of steady-state solutions in the vertical plane is undertaken in order to provide us with the necessary information to initiate the six-degrees-of-freedom continuation study.

Equations of motion

The six-degrees-of-freedom equations of motion for a submarine in surge, sway, heave, roll, pitch, and yaw, respectively, are (Smith et al 1978)

$$m[\dot{u} - vr + wq - x_G(q^2 + r^2) + y_G(pq - \dot{r}) + z_G(pr + \dot{q})] = X_H + X_W + X_C \quad (1)$$

Nomenclature

α = angle of attack
$b(x)$ = local beam of the hull
β = angle of drift
B = vehicle buoyancy
δ_B = excess buoyancy, $B - W$
δ_b = bow plane deflection
δ_r = rudder angle deflection
δ_s = stern plane deflection
$h(x)$ = local height of hull
I_x = vehicle mass moment of inertia around x-axis
(K,M,N) = roll, pitch, and yaw moments, respectively
L = vehicle length
m = vehicle mass
(p,q,r) = roll, pitch, and yaw rates, respectively
(u,v,w) = surge, sway, and heave velocities, respectively
W = vehicle weight
x_B = longitudinal position of center of buoyancy
x_G = longitudinal position of center of gravity
x_{GB} = longitudinal center of gravity/buoyancy separation, $x_G - x_B$
X_C = surge force due to control inputs
X_H = surge force due to hydrodynamics
X_W = surge force due to weight and buoyancy
(X,Y,Z) = surge, sway, and heave forces, respectively
y_G = athwartship location of center of gravity
z_B = vertical position of center of buoyancy
z_G = vertical position of center of gravity
z_{GB} = metacentric height, $z_G - z_B$
(ϕ,θ,ψ) = roll, pitch, and yaw Euler angles, respectively

$$m[\dot{v} + ur - wp + x_G(pq + \dot{r}) - y_G(p^2 + r^2) + z_G(qr - \dot{p})] = Y_H + Y_W + Y_C \quad (2)$$

$$m[\dot{w} - uq + vp + x_G(pr - \dot{q}) + y_G(qr + \dot{p}) - z_G(p^2 + q^2)] = Z_H + Z_W + Z_C \quad (3)$$

$$I_x\dot{p} + (I_z - I_y)qr + I_{xy}(pr - \dot{q}) - I_{yz}(q^2 - r^2) - I_{xz}(pq + \dot{r}) + m[y_G(\dot{w} - uq + vp) - z_G(\dot{v} + ur - wp)] = K_H + K_W + K_C \quad (4)$$

$$I_y\dot{q} + (I_x - I_z)pr - I_{xy}(qr + \dot{p}) + I_{yz}(pq - \dot{r}) + I_{xz}(p^2 - r^2) - m[x_G(\dot{w} - uq + vp) - z_G(\dot{u} - vr + wq)] = M_H + M_W + M_C \quad (5)$$

$$I_z\dot{r} + (I_y - I_x)pq - I_{xy}(p^2 - q^2) - I_{yz}(pr + \dot{q}) + I_{xz}(qr - \dot{p}) + m[x_G(\dot{v} + ur - wp) - y_G(\dot{u} - vr + wq)] = N_H + N_W + N_C \quad (6)$$

where the left-hand sides represent inertial forces and moments and the right-hand sides model the external forces. Subscript H reflects hydrodynamic contributions, W buoyancy and weight effects, C forces arising from control surface (rudders, dive planes, and bow planes) deflections, and the rest of the symbols are based on standard notation and explained in the Nomenclature.

Hydrostatic restoring forces and moments are due to the vehicle weight W and buoyancy B, and are given by

$$X_W = -(W - B)\sin\theta \quad (7)$$

$$Y_W = (W - B)\cos\theta\sin\phi \quad (8)$$

$$Z_W = (W - B)\cos\theta\cos\phi \quad (9)$$

$$K_W = (y_G W - y_B B)\cos\theta\cos\phi - (z_G W - z_B B)\cos\theta\sin\phi \quad (10)$$

$$M_W = -(x_G W - x_B B)\cos\theta\cos\phi - (z_G W - z_B B)\sin\theta \quad (11)$$

$$N_W = (x_G W - x_B B)\cos\theta\sin\phi + (y_G W - y_B B)\sin\theta \quad (12)$$

Forces and moments due to control surface deflections are reflected as added drag in surge, while in sway, heave, pitch, and yaw they are directly proportional to control surface deflection

$$X_C = uq(X_{q\delta_s}\delta_s + X_{q\delta_b}\delta_b) + X_{r\delta_r}ur\delta_r + X_{v\delta_r}uv\delta_r + uw(X_{w\delta_s}\delta_s + X_{w\delta_b}\delta_b) + u^2(X_{\delta_s\delta_s}\delta_s^2 + X_{\delta_b\delta_b}\delta_b^2 + X_{\delta_r\delta_r}\delta_r^2) \quad (13)$$

$$Y_C = Y_{\delta_r}u^2\delta_r \quad (14)$$

$$Z_C = u^2(Z_{\delta_s}\delta_s + Z_{\delta_b}\delta_b) \quad (15)$$

$$K_C = 0 \quad (16)$$

$$M_C = u^2(M_{\delta_s}\delta_s + M_{\delta_b}\delta_b) \quad (17)$$

$$N_C = N_{\delta_r}u^2\delta_r \quad (18)$$

Usually, control surface deflections are kept intentionally small, and the linearity assumption in (13) through (18) remains valid. This, of course, may not be the case in emergency scenarios and the equations should then be modified to allow for possible control surface stall. Such modifications are not included in the present model since they do not affect the qualitative features of the results, nor do they limit the applicability of the analysis techniques presented.

One of the greatest challenges in the equations of motion, (1) through (6), is the development of rational expressions for the hydrodynamic forces. The difficulty can be traced to the complex flow around a maneuvering submarine. Force and moment prediction for these flows requires accurate modeling of detailed flow phenomena such as appendage root and tip vortices, bluff-body cross-flow separation, and thick possibly separated boundary layers. These disturbances interfere with a submarine's control appendages and/or propeller, and result in responses that are often very difficult to predict. One of the most efficient computational tools capable of modeling the required flow phenomena are Reynolds averaged Navier-Stokes methods (Chen & Korpus 1992). Potential flow and/or boundary-layer theories cannot resolve the essential details of vorticity, while parabolized Navier-Stokes codes cannot handle the problem of vortex separation. In addition, one has to include what may well be the most important maneuvering influence of all, namely, viscous dominated propulsor/hull interaction forces. Unfortunately, Reynolds averaged Navier-Stokes analyses are computationally very intensive. Therefore, they can be effectively applied only for a specific numerical simulation resulting in a single trajectory prediction. Given the fact that numerical simulation results should be used with caution as they have confirmatory rather than predictive value, and the numerous combinations of initial conditions and parameter variations, one realizes that a different mechanism must be employed in order to fully and reliably establish the boundaries of the submerged operational envelope. This requirement introduces the other, equally great challenge—namely, the study of the open-loop dynamics of the equations given a particular hydrodynamic modeling. In this work we employ a traditional semi-empirical constant coefficient description. The main reason for this selection is the availability of data. Furthermore, the thrust of this work is on the nonlinear dynamics issues and not on hydrodynamic flow description. Realizing the well-known limitations of a constant coefficient hydrodynamic model, we have to establish the robustness of our results in the presence of uncertainties and inaccuracies in the values of hydrodynamic, geometric, and control surface deflections in our model. The most efficient mechanism for this is the use of recently developed methods in bifurcation and singularity theory. If we are able to recognize the bifurcation phenomena of the problem in terms of the universal unfoldings of known bifurcations, then these models will persist under finite perturbations of the parameters in the system (Golubitsky & Schaeffer 1985). The ultimate goal, of course, is the development of a framework for studying the nonlinear dynamics of a vehicle coupled with rational, nonempirical hydrodynamic computations.

Using a constant coefficient model, the hydrodynamic forces and moments are expressed as polynomial functions of the translational and rotational velocities of the vehicle with respect to the water

$$X_H = X_{pp}p^2 + X_{qq}q^2 + X_{rr}r^2 + X_{pr}pr + X_{\dot{u}}\dot{u} + X_{wq}wq + X_{vp}vp + X_{vr}vr + X_{vv}v^2 + X_{ww}w^2 - C_{D0}u^2 \quad (19)$$

$$Y_H = Y_{\dot{p}}\dot{p} + Y_{\dot{r}}\dot{r} + Y_{pq}pq + Y_{qr}qr + Y_{\dot{v}}\dot{v} + Y_{p}up + Y_{r}ur + Y_{vq}vq + Y_{wp}wp + Y_{wr}wr + Y_{v}uv + Y_{vw}vw - \frac{1}{2}\rho\int [C_{D_Y}h(x)(v + xr)^2 + C_{D_Z}b(x)(w - xq)^2]\frac{(v + xr)}{U_{cf}(x)}dx \quad (20)$$

$$Z_H = Z_{\dot q}\dot q + Z_{pp}p^2 + Z_{pr}pr + Z_{rr}r^2 + Z_{\dot w}\dot w + Z_q uq + Z_{vp}vp + Z_{vr}vr + Z_{uw}uw + Z_{vv}v^2 - \frac{1}{2}\rho \int [C_{D_Y}h(x)(v + xr)^2 + C_{D_Z}b(x)(w - xq)^2]\frac{w - xq}{U_{cf}(x)}dx \quad (21)$$

$$K_H = K_{\dot p}\dot p + K_{\dot r}\dot r + K_{pq}pq + K_{qr}qr + K_{\dot v}\dot v + K_p up + K_r ur + K_{vq}vq + K_{wp}wp + K_{wr}wr + K_v uv + K_{vw}vw \quad (22)$$

$$M_H = M_{\dot q}\dot q + M_{pp}p^2 + M_{pr}pr + M_{rr}r^2 + M_{\dot w}\dot w + M_q uq + M_{vp}vp + M_{vr}vr + M_{uw}uw + M_{vv}v^2 + \frac{1}{2}\rho \int [C_{D_Y}h(x)(v + xr)^2 + C_{D_Z}b(x)(w - xq)^2]\frac{(w - xq)}{U_{cf}(x)}xdx \quad (23)$$

$$N_H = N_{\dot p}\dot p + N_{\dot r}\dot r + N_{pq}pq + N_{qr}qr + N_{\dot v}\dot v + N_p up + N_r ur + N_{vq}vq + N_{wp}wp + N_{wr}wr + N_v uv + N_{vw}vw - \frac{1}{2}\rho \int [C_{D_Y}h(x)(v + xr)^2 + C_{D_Z}b(x)(w - xq)^2]\frac{(v + xr)}{U_{cf}(x)}xdx \quad (24)$$

The cross-flow integral terms are integrated over the length of the body and they model quadratic drag forces. The cross-flow velocity U_{cf} is

$$U_{cf} = [(v + xr)^2 + (w - xq)^2]^{1/2} \quad (25)$$

The hydrodynamic coefficients in the above equations are assumed to be independent of vehicle speed, which is a relatively accurate approximation. A more important assumption is that they are also assumed to be constant throughout the range of vehicle angles of drift and attack. Ordinary maneuvering models are usually validated for angles of attack between ±15 deg. For higher angles, the cross-flow drag terms C_{D_Y} and C_{D_Z} dominate the response and they are functions of the side slip angle or angle of attack. For this reason, the results will have to be carefully interpreted for large angles of attack. Incorporation of angle-of-attack dependence, however, should not affect significantly the qualitative bifurcation characteristics of our results. The reason for this is that universal bifurcation unfoldings are robust with regard to parameter variations and model uncertainties.

Finally, the kinematic equations express the rates of change of the Euler angles (ϕ,θ,ψ) in terms of the vehicle orientation and angular velocities as in

$$\dot\phi = p + q\sin\phi\tan\theta + r\cos\phi\tan\theta \quad (26)$$

$$\dot\theta = q\cos\phi - r\sin\phi \quad (27)$$

$$\dot\psi = q\frac{\sin\phi}{\cos\theta} + r\frac{\cos\phi}{\cos\theta} \quad (28)$$

We assume that propulsion is inoperative and the vehicle propeller is rotating freely. The driving mechanism for vehicle motions is the amount and location of excess buoyancy. The problem then is to establish the dynamics of the system in such a condition.

Vertical plane solutions

Steady-state solutions are characterized by the conditions

$$\dot u = \dot v = \dot w = \dot p = \dot q = \dot r = \dot\phi = \dot\theta = 0 \quad (29)$$

Substituting (29) into the equations of motion yields a highly nonlinear coupled system of eight equations in the eight unknown state variables, u, v, w, p, q, r, ϕ, and θ at steady state. Such a system may admit, of course, a multitude of solutions depending on the initial conditions. In order to obtain the necessary initial estimates for the six-degrees-of-freedom continuation analysis, we make the additional assumption $\dot\psi = 0$ at steady state. This forces a constant yaw angle at equilibrium and, as a result, it restricts the nominal equilibrium set in the vertical plane. The two necessary, but not sufficient, conditions for steady-state motion to be restricted in the vertical plane are (Papoulias & McKinley 1994) rudder at zero:

$$\delta_r = 0$$

and center-of-gravity/buoyancy "symmetry" with respect to the centerplane:

$$y_G W - y_B B = 0$$

The steady-state conditions (29) then reduce to a single equation for the dimensionless heave velocity, $x = w/u$

$$x|x| + \beta x^2 + \lambda x + \alpha = 0 \quad (30)$$

where we have assumed that only positive solutions in u are admitted. Once equation (30) is solved, the remaining state variables are single-valued functions of x (Papoulias & McKinley 1994). The coefficients β, λ, and α of (30) are given in terms of our physical parameters as

$$\beta = \frac{p_z X_{ww}}{C_{D_Z}A_w(p_x + x_A\delta_B)}$$

$$\lambda = \frac{M_w\delta_B - p_x Z_w + p_s(X_{w\delta_s}\delta_s + X_{w\delta_b}\delta_b)}{C_{D_Z}A_w(p_x + x_A\delta_B)}$$

$$\alpha = \frac{\delta_B(M_{\delta_s}\delta_s + M_{\delta_b}\delta_b) + p_z(X_{\delta_s\delta_s}\delta_s^2 + X_{\delta_b\delta_b}\delta_b^2 - C_{D0}) + p_x(Z_{\delta_s}\delta_s + Z_{\delta_b}\delta_b)}{C_{D_Z}A_w(p_x + x_A\delta_B)} \quad (31)$$

where

$$A_w = \int b(x)dx$$

$$x_A = \frac{1}{A_w}\int xb(x)dx$$

$$p_x = x_{GB}W - x_B\delta_B$$

$$p_z = z_{GB}W - z_B\delta_B$$

$$x_{GB} = x_G - x_B$$

$$z_{GB} = z_G - z_B$$

$$\delta_B = B - W$$

and $b(x)$ is the local beam of the hull.

Analysis of the solution set of (30) in terms of singularity theory can be accomplished by rewriting it as

$$x|x| + (\lambda_0 + \lambda_1\delta)x + (\alpha_0 + \alpha_1\delta + \alpha_2\delta^2) + \beta x^2 = 0$$

$$\text{or} \qquad G(x,\delta,p_1,p_2) = 0 \quad (32)$$

where we have adopted the dive plane angle δ as our primary bifurcation parameter. The remaining variables in (32) are expressed in terms of the new unfolding parameters

$$p_1 = \frac{\delta_B}{p_x + x_A \delta_B} \tag{33}$$

$$p_2 = \frac{p_z}{p_x + x_A \delta_B} \tag{34}$$

where

$$\lambda_0 = -\frac{Z_w}{C_{D_Z} A_w} + \frac{M_w + x_A Z_w}{C_{D_Z} A_w} p_1$$

$$\lambda_1 = \frac{X_{w\delta_s} + X_{w\delta_b}\alpha_\delta}{C_{D_Z} A_w} p_2$$

$$\alpha_0 = -\frac{C_{D0}}{C_{D_Z} A_w} p_2$$

$$\alpha_1 = -\frac{Z_{\delta_s} + Z_{\delta_b}\alpha_\delta}{C_{D_Z} A_w} + \frac{M_{\delta_s} + M_{\delta_b}\alpha_\delta + x_A(Z_{\delta_s} + Z_{\delta_b}\alpha_\delta)}{C_{D_Z} A_w} p_1$$

$$\alpha_2 = \frac{X_{\delta_s\delta_s} + X_{\delta_b\delta_b}\alpha_\delta^2}{C_{D_Z} A_w} p_2$$

$$\beta = \frac{X_{www}}{C_{D_Z} A_w} p_2$$

and

$$\alpha_\delta = \frac{\delta_b}{\delta_s}$$

is the bow plane to dive plane ratio. The purpose of the analysis in this section is to classify the geometry of the solutions of (32) for any physically realizable range of variations of the parameters δ, p_1, and p_2.

Since we seek to characterize vertical plane solutions before we attempt six-degrees-of-freedom computations, we start first with the degenerate case when $p_z = 0$. The physical significance of the degeneracy condition $p_z = 0$ is simply $z_G W = z_B B$. In such a case, $p_2 = 0$, and (32) becomes

$$x|x| + \lambda_0 x + \alpha_1 \delta = 0 \quad \text{or} \quad g(x,\delta,p_1) = 0 \tag{35}$$

Equation (35) represents a typical hysteresis bifurcation. Hysteresis occurs when $g = g_x = g_{xx} = 0$, which implies that $\lambda_0 = 0$. When $\lambda_0 > 0$, $g_x \neq 0$ always and the solution set of $g = 0$ is a single-valued function in δ. Onset of hysteresis occurs for $\lambda_0 = 0$, which results in

$$x_{GB} = \frac{M_w + x_B Z_w}{Z_w W} \delta_B \tag{36}$$

When $\lambda_0 < 0$ a hysteresis loop exists for a certain range of δ. This is computed from $g = g_x = 0$, or

$$\lambda_0^4 - 16\alpha_1^2\delta^2 = 0 \tag{37}$$

Between the two values of δ specified by (37), equation (35) has three solutions, two of which are stable and the central one unstable. Equation (37) represents a cuspoid curve symmetric with respect to the $\alpha_1\delta = 0$ axis with the cusp located at the origin. For negative λ_0 and for values of $\alpha_1\delta$ located inside the cusp (37), equation (35) admits three solutions in x. The above results are presented graphically in Fig. 2.

The hysteresis bifurcation (35) does not persist when $p_z \neq 0$. In such a case, the generic solution set is described by (32), which takes the form of the winged cusp singularity (Golubitsky & Schaeffer 1985). The set of the hysteresis points

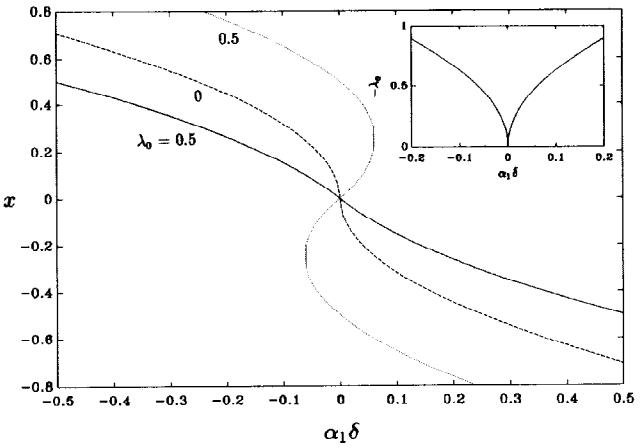

Fig. 2 Degenerate hysteresis solution set and cusp curve

of (32), $\mathcal{H}$, can be computed from the simultaneous solution of

$$G = G_x = G_{xx} = 0 \tag{38}$$

Explicit determination of the derivatives in (38) yields the condition

$$\alpha_0\lambda_1^2 - \alpha_1\lambda_0\lambda_1 + \alpha_2\lambda_0^2 = 0 \tag{39}$$

which describes the hysteresis set in a (p_1,p_2) parameter space. Multiple solutions of (32) are generated along the bifurcation set $\mathcal{B}$ which is computed by solving

$$G = G_x = G_\delta = 0 \tag{40}$$

This results in the following cusplike curve

$$[\text{sgn}(x) + \beta](\alpha_1 + 2\alpha_2\delta)^2 - \lambda_1(\lambda_0 + \lambda_1\delta)(\alpha_1 + 2\alpha_2\delta) + \lambda_1(\alpha_0 + \alpha_1\delta + \alpha_2\delta^2) = 0 \tag{41}$$

where

$$\delta = \frac{2[\text{sgn}(x) + \beta]\alpha_1 - \lambda_0\lambda_1}{\lambda_1^2 - 4\alpha_2[\text{sgn}(x) + \beta]}$$

and $\text{sgn}(x) = +1$ if $x > 0$, and $\text{sgn}(x) = -1$ if $x < 0$. Depending on the number of physical parameters that are employed in a particular problem, equations (39) and (41) describe curves or higher dimensionality surfaces in the appropriate parameter space. Schematically, this is represented in Fig. 3 along with typical shapes of solution sets x versus δ for various parameter domains. Actual solution sets of (32) for $\lambda_1 = \alpha_0 = \alpha_1 = \beta = 0$, $\alpha_2 = 1$, and different values of λ_0 are presented in Fig. 4.

Typical solution sets for the SDV and for physically realizable ranges of the parameters produce graphs that are subsets, in a qualitative sense, of Figs. 3 and 4 (Papoulias & McKinley 1994). The practical implications of the results of this section is that they provide us with a *complete* description of the geometry of all possible steady-state solutions in the vertical plane. Equipped with such a capability, we can now proceed with the analysis of out-of-plane solutions using numerical continuation and singularity theory methods.

Out-of-plane solutions

The in-plane solutions studied in the previous section are valid only under the prescribed symmetry conditions $\delta_r = 0$

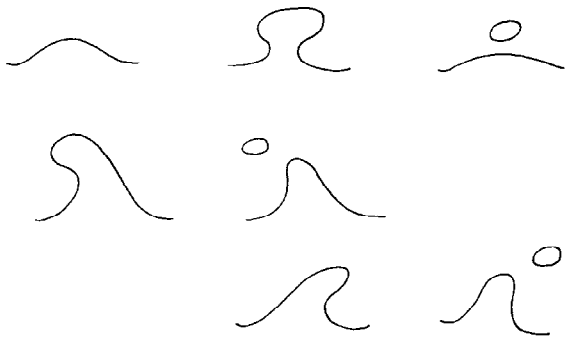

Fig. 3 Persistent perturbations of winged cusp singularity

and $y_G W - y_B B = 0$. As a result they are quite nonpersistent, and small asymmetric perturbations can easily perturb them into general out-of-plane motions. The latter could also be observed even under the above symmetric conditions both in experiments (Booth 1977) and simulations (McKinley 1991). General out-of-plane solutions can be computed by solving the following system of six coupled algebraic equations in the six unknowns u, v, w, ϕ, θ, and $\dot{\psi}$:

$$m[-vr + wq - x_G(q^2 + r^2) + y_G pq + z_G pr] = X_H + X_W + X_C \quad (42)$$

$$m[ur - wp + x_G pq - y_G(p^2 + r^2) + z_G qr] = Y_H + Y_W + Y_C \quad (43)$$

$$m[-wq + vp + x_G pr + y_G qr - z_G(p^2 + q^2)] = Z_H + Z_W + Z_C \quad (44)$$

$$(I_z - I_y)qr + I_{xy}pr - I_{yz}(q^2 - r^2) - I_{xz}pq + m[y_G(-uq + vp) - z_G(ur - wp)] = K_H + K_W + K_C \quad (45)$$

$$(I_x - I_z)pr - I_{xy}qr + I_{yz}pq + I_{xz}(p^2 - r^2) - m[x_G(-uq + vp) - z_G(-vr + wq)] = M_H + M_W + M_C \quad (46)$$

$$(I_y - I_x)pq - I_{xy}(p^2 - q^2) - I_{yz}pr + I_{xz}qr + m[x_G(ur - wp) - y_G(-vr + wq)] = N_H + N_W + N_C \quad (47)$$

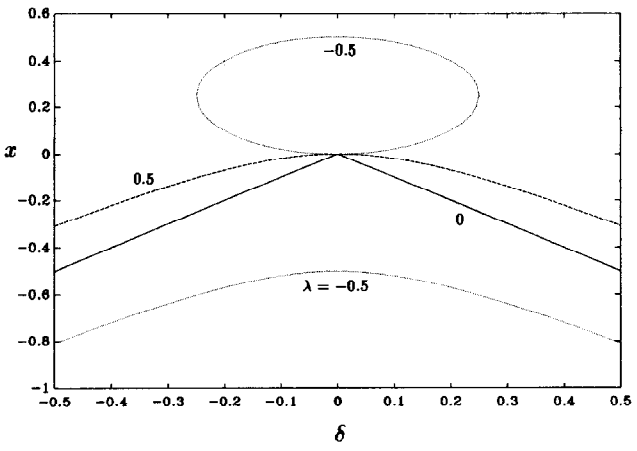

Fig. 4 Solution set x versus δ for $\lambda_1 = \alpha_0 = \alpha_1 = \beta = 0$, $\alpha_2 = 1$, and different values of λ_0

The angular velocities p, q, and r in (42) through (47) are functions of $\dot{\psi}$, ϕ, and θ and are obtained from (26) through (27) by substituting $\dot{\phi} = \dot{\theta} = 0$:

$$p = -\dot{\psi}\sin\theta$$
$$q = \dot{\psi}\sin\phi\cos\theta$$
$$r = \dot{\psi}\cos\phi\cos\theta \quad (48)$$

It should be mentioned that we explicitly allow $\dot{\psi} \neq 0$ so that motion takes place in six degrees of freedom. Substitution of $\dot{\psi} = 0$ in (48) yields $p = q = r = 0$, and equations (42) to (47) then produce the vertical plane solutions of the previous section.

The challenge in solving (42) through (47) is to ensure that all meaningful solutions are computed for a given physically realizable range of variation of the parameters for which the model is valid. To this end, we utilized the following three-stage approach:

1. The analytical results for vertical plane motions are used as initial approximations for the more general case of six-degrees-of-freedom motions. Additional information is provided through a limited set of carefully selected numerical integrations in cases where loss of stability in the vertical plane is detected.
2. Stability analysis of vertical plane solutions identifies parameter values where out-of-plane solution branching may occur. Detailed local search in the neighborhood of these critical parameter values is then initiated in order to obtain initial approximations for these out-of-plane motions.
3. In cases where the prescribed symmetry conditions, $\delta_r = 0$ and $y_G W - y_B B = 0$, are not satisfied, an incremental technique is utilized. First, the vertical plane solution is obtained. The asymmetry condition is then slightly introduced and the new out-of-plane solution is computed using the previous solution as initial approximation. The process is repeated until the full asymmetry condition is applied.

Combination of the above three steps assures that all meaningful solutions are captured. The actual numerical vehicle which performs the indicated computations in the above organizational scheme is continuation (Seydel 1988). The principles of continuation are based on homotropy techniques where a problem is embedded into a larger class of problems which are parametrized by a single distinguishing parameter. This class is then solved by systematically varying the parameter within a specified range using first a predictor and then a corrector algorithm, as is schematically depicted in Fig. 5. The primary advantage of continuation is that it can easily trace solution branches through bifurcation and turning points. It should be pointed out however, that we were able to reproduce the continuation results by using standard IMSL (International Mathematical and Statistical Libraries) nonlinear solvers; the disadvantage is that

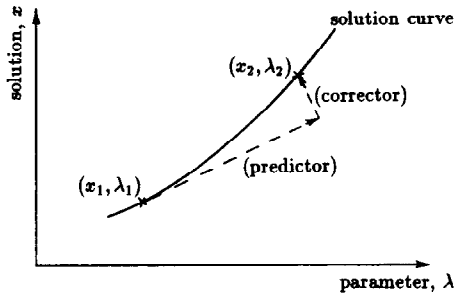

Fig. 5 Principles of continuation

a simple step-through approach breaks down when a turning point is encountered.

Although the steady-state analysis described above can compute all possible steady-state solutions, it gives no indication as to which of the solutions are stable. Dynamic stability of the equations of motion can be easily assessed once a steady-state solution has been found. This is accomplished by linearization (Guckenheimer & Holmes 1983) in the neighborhood of the desired solution. The eigenvalues of the Jacobian matrix of the first partial derivatives of our nonlinear vector field evaluated at the nominal point are computed. If all eigenvalues have negative real parts, the indicated steady-state solution is asymptotically stable, while if at least one eigenvalue has a positive real part, the nominal solution is unstable. In the following section we concentrate our attention on physically meaningful solutions, and attempt to classify those solutions that are either stable or perturb into stable steady states.

Steady-state solutions

In this section we present in a systematic way typical steady-state results with variations in the dive plane angle δ_s, rudder angle δ_r, amount of excess buoyancy δ_B, location of excess buoyancy x_{GB}, and metacentric height z_{GB}. The primary conclusion of this section is that loss of stability occurs in the form of a multiparameter pitchfork bifurcation. Recognition of this bifurcation is accomplished by suitable projections on two-dimensional parameter planes discussed below.

Variations in δ_s: the pitchfork and separation

Extensive computations in the vertical plane reported in Papoulias & McKinley (1994) suggest that there exists a certain combination of the parameters (δ_s, x_{GB}) where the in-plane solution becomes unstable as a result of one real eigenvalue of the linearized system matrix crossing zero. A systematic numerical search employing the continuation principles described in the previous section revealed the existence of a generic pitchfork bifurcation. Typical results are presented in Figs. 6 and 7, where we show the drift angle β and angle of attack α versus δ_s for different values of the rudder angle δ_r, all in degrees. For these results we used $\delta_B = 2\%W$, $z_{GB} = 0.1$ ft, and $x_{GB} = -1\%L$. Results for different parameter values are qualitatively similar to the results presented here. Stable (S) and unstable (U) solutions are indicated on the graphs. It should be mentioned that the vastly different behavior for $\delta_s < 0$ and $\delta_s > 0$ is due to the negative

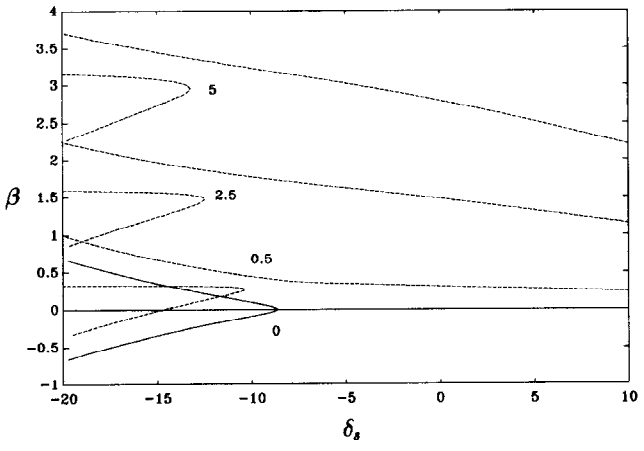

Fig. 6 Angle of drift versus δ_s for different values of δ_r (deg)

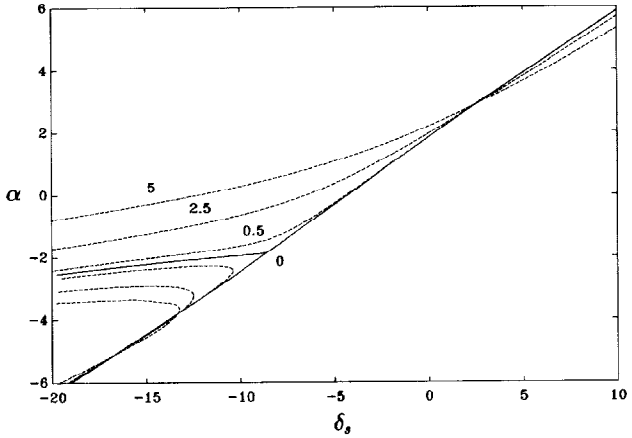

Fig. 7 Angle of attack versus δ_s for different values of δ_r (deg)

value of x_{GB}, i.e., center of buoyancy forward of the center of gravity. The pitchfork bifurcation occurs generically in nonlinear dynamical systems where, besides the zero crossing real eigenvalue condition, a reflectional symmetry $x \to -x$ of the vector field exists (Guckenheimer & Holmes 1983). Since for $\delta_r = 0$ our system is clearly symmetric with respect to the horizontal plane variables v, r, p, and ϕ, the occurrence of the pitchfork follows. At the critical point of bifurcation, the stability of the trivial equilibrium changes, and a new pair of equilibria related by the symmetry appears to one side of the critical point in the parameter space, as shown in Fig. 6. The behavior of all horizontal plane variables is qualitatively similar to that of the drift angle β. The nominal in-plane solution $\beta = 0$ becomes unstable at a certain value of δ_s, and a pair of symmetric out-of-plane solutions $\beta \neq 0$ appears. These solutions are locally stable. For nonzero values of δ_r, the reflectional symmetry exhibited by the equations is destroyed, and the pitchfork bifurcation assumes its persistent perturbed form demonstrated in the figure. The bifurcation point where multiple solutions are generated moves now to a lower value of δ_s as δ_r is increased in absolute value. The two outer solutions are stable while the inner solution is unstable. This is known as the saddle-node bifurcation since at the bifurcation point, one stable equilibrium (a node) coalesces with an unstable one (a saddle), resulting in their mutual destruction. Negative values of δ_r produce steady-state solutions that are simply reflected with respect to the $\beta = 0$ axis. Vertical plane results are shown in Fig. 7 in terms of the angle of attack α. Since the vertical plane variables u, w, q, and θ are, for $\delta_r = 0$, even functions of the horizontal plane variables, the (α,δ_s) diagram exhibits a form of solution separation and does not distinguish between port and starboard out-of-plane motions. For nonzero δ_r the results are perturbed as expected. As a final observation, it can be seen that the results shown in the previous two figures involve quite small angles of drift and attack, which means that the constant coefficient hydrodynamic model remains valid.

This pitchfork bifurcation can be qualitatively described by the one-parameter family

$$f(x,\lambda) = x^3 + \lambda x + \gamma \tag{49}$$

where x signifies any one of the horizontal plane variables v, r, p, and ϕ. The primary bifurcation parameter is λ, which physically corresponds to the dive plane angle δ_s through some continuous nonlinear transformation. The rudder angle δ_r is

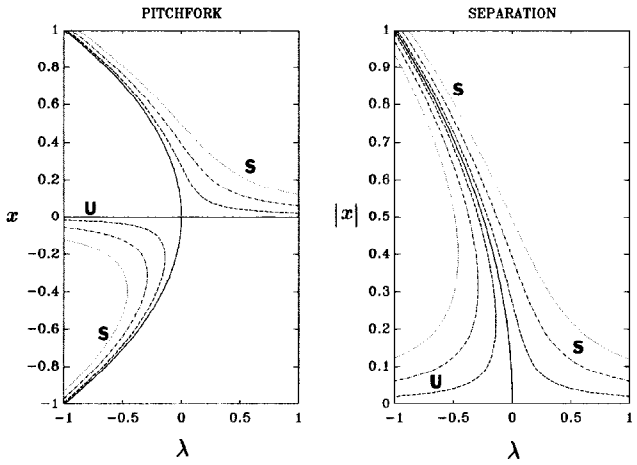

Fig. 8 Schematic diagrams of pitchfork and separation bifurcation

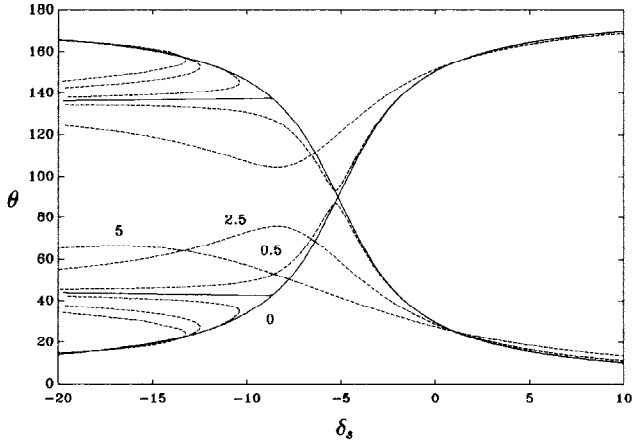

Fig. 10 Pitch angle versus δ_s for different values of δ_r (deg)

mapped via a one-to-one transformation to the mathematical unfolding parameter γ. Symbolically, we can represent this by writing

$$\delta_s \rightarrow \lambda, \quad \text{and} \quad \delta_r \rightarrow \gamma \tag{50}$$

For the unperturbed problem, $\gamma = 0$, we can see that $f(x,\lambda) = 0$ admits only one solution, $x = 0$, for $\lambda > 0$ and three solutions, $x = 0$ and $x = \pm\sqrt{-\lambda}$, for $\lambda < 0$. Solution sets (x,λ) for zero and nonzero values of γ are shown in Fig. 8 where the qualitative similarities with the actual results of Fig. 6 are evident; namely, there exists a critical point where the primary solution branch loses its stability and it bifurcates into two stable out-of-plane branches. In case that another variable in the system, y, is an even function of x, say $y = |x|$, we get the separation solution diagrams also shown in Fig. 8. Physically, y corresponds to our vertical plane state variables, as is evident from the similarities between Figs. 8 and 7.

With the aid of the pitchfork bifurcation diagrams we can explain the pathological simulation results presented in Fig. 1. Figure 9 presents the steady-state roll angle ϕ versus δ_s with δ_r as the parameter. An interesting behavior is exhibited near the bifurcation point for small values of δ_r. The

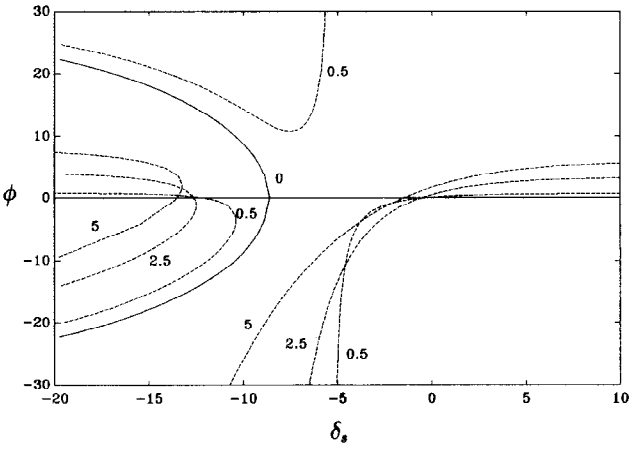

Fig. 9 Roll angle versus δ_s for different values of δ_r (deg)

solutions in ϕ diverge away from their zero values and are attracted by the complementary solutions that are located close to $\phi = \pi$. It appears therefore that the exact solution set of ϕ is very sensitive in this range to the precise values of the parameters used in the model as well as to the external disturbances. Any results obtained by numerical simulations of this model in such a range of parameters should be viewed with extreme caution. This is true for small values of δ_r, while larger values of rudder angle result in steady-state roll angles that are located "close" to zero throughout the range of δ_s. Therefore, for a certain band of δ_s around -5 deg, smaller rudder angles result in larger angles of roll and vice versa. The situation is, of course, reversed for most of the range of δ_s, as expected.

Figure 10 presents results in terms of the pitch angle θ versus δ_s for different values of δ_r. The resulting angles of attack were very small throughout the range of bifurcation phenomena in this and all similar figures of this section. Both steady-state solutions, θ and its complementary $\pi - \theta$, are shown. Inverted pendulum stabilization can be seen to occur for values of δ_s less than approximately -5 deg. The results of Fig. 10 demonstrate that, in certain cases, the inverted pendulum stabilization studied in Papoulias & McKinley (1994) is highly degenerate as it applies only for $\delta_r = 0$. Small nonzero rudder angles cause solution veering instead of solution crossing, and as a result the steady-state pitch angle is always less than 90 deg. This is of course specific to these particular results; other cases of inverted pendulum stabilization are shown to persist even under the asymmetry generated by nonzero rudder angles (Aydin 1993).

Variations in δ_r: hysteresis branches and teardrops

As Figs. 6 through 10 demonstrate, there exists a certain range of the parameters δ_s and δ_r such that the number of steady-state solutions changes from one to three. This effect can be seen more clearly by admitting δ_r as our primary continuation parameter and δ_s as our perturbation parameter. Typical results in terms of the angular velocity in yaw, r, are shown in Fig. 11 and in terms of the angle of attack in Fig. 12. It can be seen that for a certain range of δ_s the solution set is a single-valued function of r or α for the entire range of δ_r. Beyond a certain value of δ_s, however, there exists a range of δ_r where the solution set is a triple-valued function in δ_r. Of the three solutions, the two outer are stable while the inner is unstable. This is a typical hysteresis diagram, and discontinuous jumps in the steady-state solu-

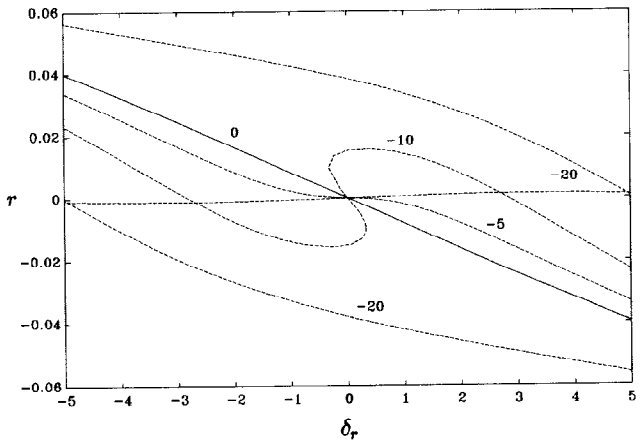

Fig. 11 Yaw angular velocity (rad/sec) versus δ_r (deg) for different values of δ_s (deg)

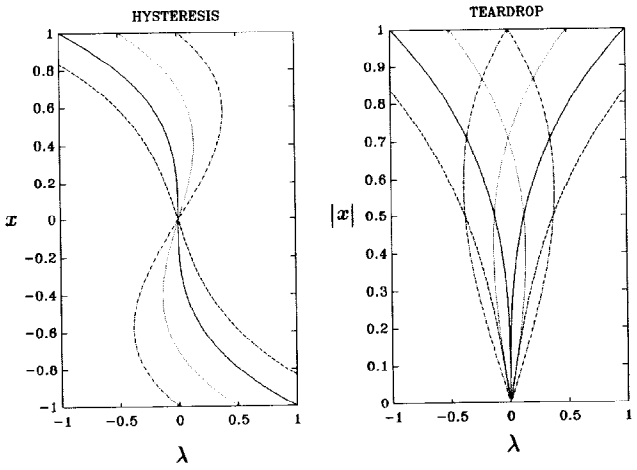

Fig. 13 Schematic diagrams of hysteresis and teardrop bifurcation

tion structure can be experienced in practice upon continuous variations of the rudder angle.

Hysteresis bifurcations can be described by a simple model similar to (49)

$$f(x,\lambda) = x^3 + \gamma x + \lambda \tag{51}$$

with the exception that the roles of λ and γ are interchanged:

$$\delta_r \to \lambda, \quad \text{and} \quad \delta_s \to \gamma \tag{52}$$

In Fig. 13 we plot x versus the primary bifurcation parameter λ for different values of the unfolding parameter γ. Again, it can be seen that the simple model captures the essential structure of the solution set very well. Typical hysteresis diagrams develop for the horizontal plane variables, whereas the vertical plane variables are even functions in x and they exhibit typical structures in the shape of teardrops as seen in the figures. For certain ranges of the parameters (λ,γ) or, equivalently, (δ_r,δ_s), a closed branch of additional solutions in a vertical plane variable is generated and is being shed off the primary solution branch as the parameters move farther away from the bifurcation point.

Variations in δ_B: the terminal pitchfork

A plot of the steady-state surge velocity u, with the amount of excess buoyancy δ_B as the primary bifurcation parameter, is shown in Fig. 14. The value of the rudder angle, δ_r, is kept at zero for these results, which means that we are studying symmetric solutions. The perturbation parameter is the dive plane angle δ_s, while we keep $z_{GB} = 0.1$ ft and $x_{GB} = -1\%L$. We observe the following qualitative features of the results:

1. For $\delta_s = 0$ there exist two in-plane solutions in u. One is of relatively low value and is unstable. The other has a higher value and is the stable solution.
2. This distinction between a stable predominantly forward motion and an unstable nearly vertical ascent becomes more pronounced as the dive plane angle increases to -5 deg, but it becomes less pronounced as δ_s is further increased to -20 deg.
3. For $\delta_s = -20$ the predominantly forward motion loses its stability before it coalesces with the nearly vertical ascent, exhibiting a typical solution separation with a bifurcation into out-of-plane motions.

We will refer to the particular pitchfork behavior shown in Fig. 14 as the terminal pitchfork. The reason for this ter-

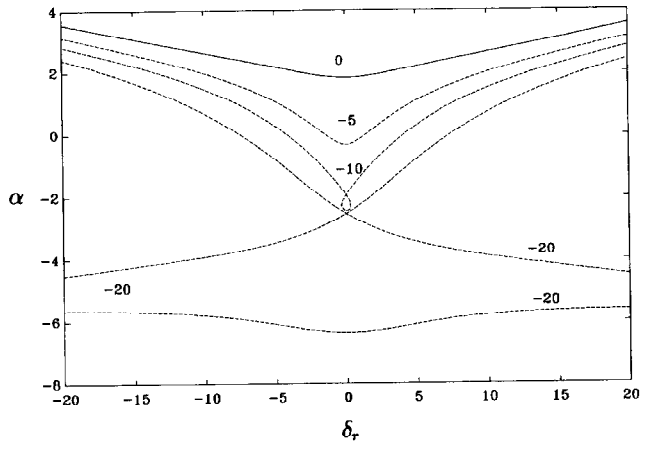

Fig. 12 Angle of attack versus δ_r for different values of δ_s (deg)

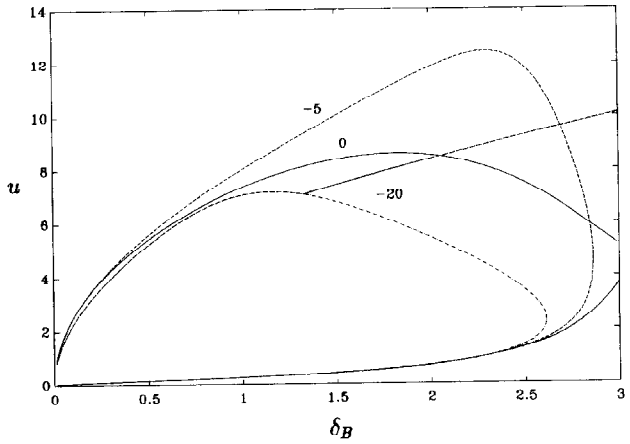

Fig. 14 Surge velocity (ft/sec) versus excess buoyancy (%W) for $\delta_r = 0$ and different values of δ_s (deg)

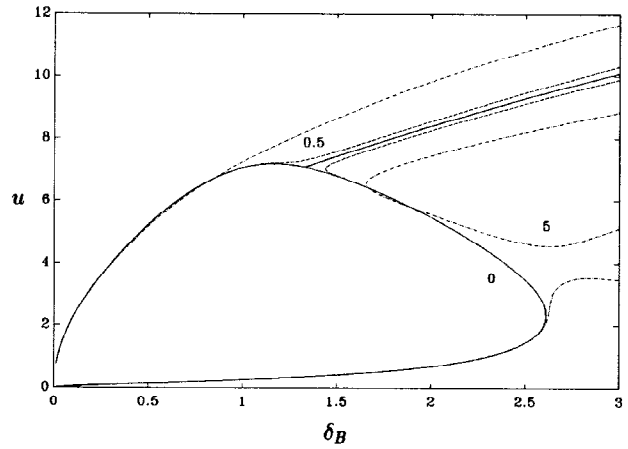

Fig. 15 Surge velocity (ft/sec) versus excess buoyancy (%W) for $\delta_s = -20$ and different values of δ_r (deg)

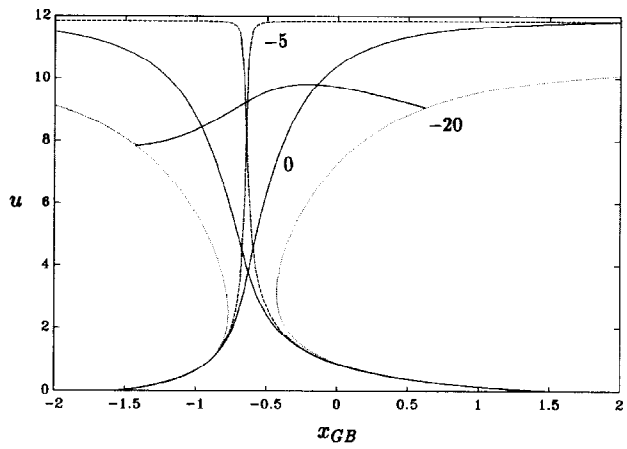

Fig. 17 Surge velocity (ft/sec) versus x_{GB}(%L) for different values of δ_s (deg) and for $\delta_r = 0$

minology is the fact that depending on the value of δ_s, there exists a certain value of δ_B where the primary in-plane solution branch disappears. The secondary out-of-plane solution branches are persistent throughout the range of δ_B considered. The effects of asymmetry are shown in Fig. 15 where we present (u,δ_B) for $\delta_s = -20$ (deg) and for different values of δ_r, in degrees. Typical biased solution separation is exhibited near the pitchfork point, as expected. Another interesting feature is observed for high values of δ_r where the primary solution curve dissolves into two separate solution branches near the initial pitchfork terminal point. Both of these separate solutions are unstable. The stable solutions are the two primary out-of-plane branches that emanate from the initial separation point.

A plot of the roll angle (ϕ,δ_B) is shown in Fig. 16 for the same conditions used in Fig. 15. The pitchfork terminal point can be clearly seen. Also we observe, as before, that solution divergence and extreme sensitivity to initial conditions can be expected for parameter values prior to the pitchfork bifurcation point. The mechanism responsible for this is the existence of the inverted pendulum solution, $(\pi - \phi)$, which locally can attract solution branches, as explained before.

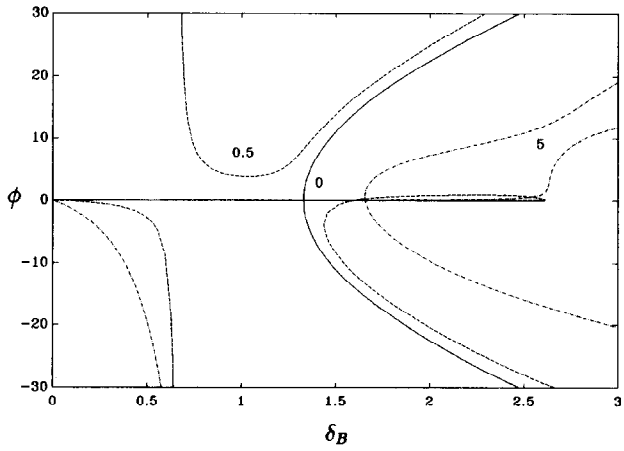

Fig. 16 Roll angle (deg) versus excess buoyancy (%W) for $\delta_s = -20$ and different values of δ_r (deg)

Variations in x_{GB}: multiple connected pitchforks

A plot of the surge velocity (ft/sec) using x_{GB} as the primary continuation parameter is shown in Fig. 17. For these results, the dive plane angle δ_s serves as the perturbation parameter, and the rest of the parameters are held constant at $\delta_B = 2\%W$, $z_{GB} = 0.1$ ft, and $\delta_r = 0$. Two distinct solutions can be seen for $\delta_s = 0$; these are identified as predominantly forward motion and nearly vertical ascent at the extremes of the range of x_{GB}, while for intermediate x_{GB} values the actual steady-state motion is a combination of the two. Which solution is stable depends on the particular value of x_{GB} (McKinley 1991, Aydin 1993). Both solutions are in-plane solutions. As the dive plane angle δ_s changes from 0 to -5 we observe that the two in-plane solutions come closer together and the distinction between predominantly forward motion and nearly vertical ascent becomes more pronounced. Further reductions in δ_s cause the two in-plane solutions to become separated and we can observe the generation of an out-of-plane solution connecting them. This corresponds to a couple of multiple connected pitchfork bifurcations at x_{GB} values approximately $-1.4\%L$ and $0.6\%L$ as shown in the figure. It can be seen that for certain combinations of (x_{GB},δ_s) no stable in-plane solution exists, and the steady-state motion is out-of-plane. The trivial solution of the corresponding pitchfork bifurcation ceases to exist in this case, and the only solutions remaining are the two symmetric secondary branches joining the two pitchfork points.

It should be pointed out that the numerical results cannot be validated for the cases of very small surge velocity since these correspond to high angles of attack which are outside the range of validity of the hydrodynamic model. However, since we unfold each bifurcation properly, we expect the above results to be qualitatively correct throughout the ranges of parameter variations that are presented. Typical results for the asymmetric multiple connected pitchfork bifurcation are shown in Fig. 18 for $\delta_s = -20$ deg and different values of δ_r in degrees. Comparing Figs. 17 and 18, we can see that the effect of the asymmetry introduced by $\delta_r \neq 0$ is to deform the solution set while its qualitative features remain the same. The symmetric steady-state results of Fig. 17 are "shaken up" to unfold the asymmetric results shown in Fig. 18. Naturally, all solutions in this case correspond to out-of-plane motions. Comparing the results presented in these two figures, we can easily establish which out-of-plane solutions will result in predominantly vertical plane response and which ones will allow large excursions in six degrees of freedom.

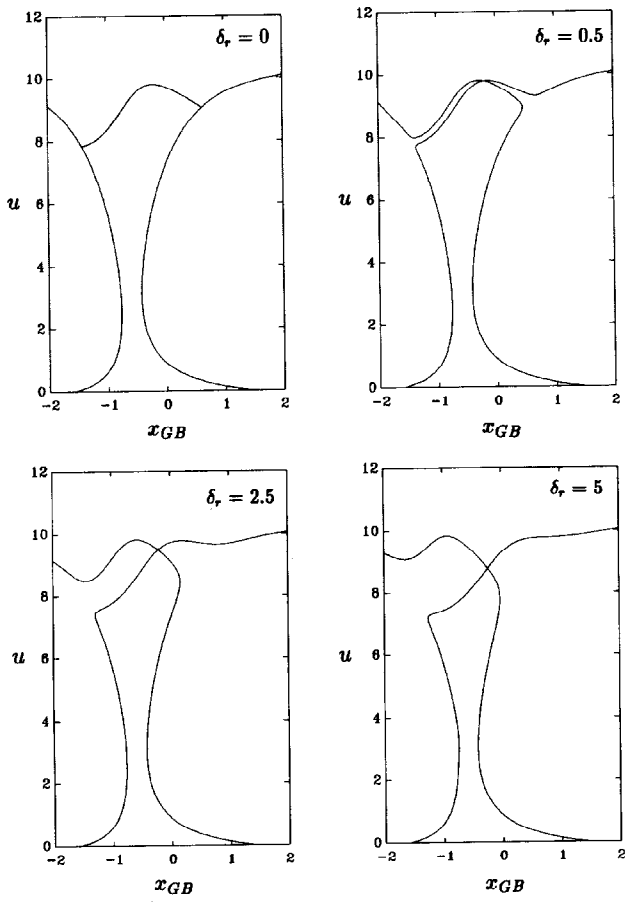

Fig. 18 Surge velocity (ft/sec) versus $x_{GB}(\%L)$ for $\delta_s = -20$ (deg) and different values of δ_r (deg)

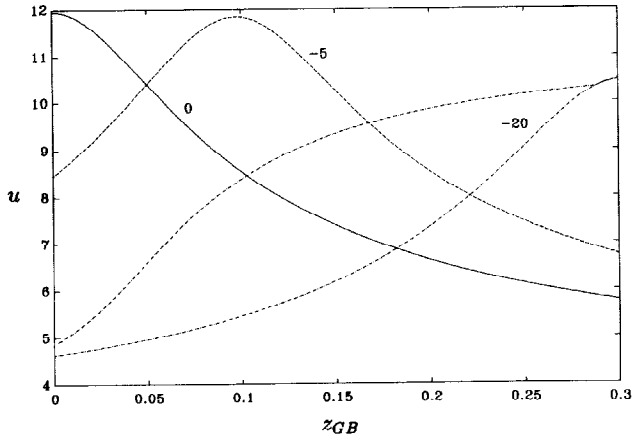

Fig. 19 Surge velocity (ft/sec) versus z_{GB} (ft) for $\delta_r = 0$ and different values of δ_s (deg)

Variations in z_{GB}: double pitchforks

As a final set of results, we present two typical plots (u,z_{GB}), i.e., using the metacentric height as the primary continuation parameter. Results for $\delta_r = 0$ and different values of δ_s are shown in Fig. 19. A characteristic pitchfork bifurcation is presented for two different values of z_{GB} and for values of δ_s beyond a certain critical value. For the pitchfork case, $\delta_s = -20$ deg, the upper solution branch corresponds to the two out-of-plane solutions, while the lower branch is the in-plane predominantly forward motion. The effects of asymmetry on this double pitchfork are presented in Fig. 20, where the graph of (u,z_{GB}) is produced for $\delta_s = -20$ deg and different values of δ_r. The existence of two pitchforks at two distinct values of the metacentric height is evident from this graph.

Bifurcation graphs

Symmetric cusp catastrophe curves and path formulations

Consider an equilibrium state of our system depending on the two parameters (δ_s,δ_r) and assume that, in some domain of variation of these parameters, this equilibrium state does not bifurcate. We can describe the system by a point in the parameter space, that is, a point corresponding to the parameter value on the parameter plane (δ_s,δ_r). We consider a division of this parameter plane into two open and disjointed parts depending on whether the equilibrium state is stable or not. In our case, since we are focusing on static bifurcations, this is equivalent to whether the number of equilibrium states changes or not. Thus we obtain on the plane of parameters two distinct domains characterized by the number and stability properties of equilibrium states. Separating the two domains are the stability boundaries. Generically, upon projection of a smooth surface onto a plane, the resulting contour has two kinds of singularities. These are the cusp, a discontinuity in the first derivative, and a fold which is smooth throughout. All other singularities disintegrate under small movements of the surface and/or the angle of projection while these two types are stable and persist under small deformations of the mapping.

An analytic representation of the cusp curve can be found by considering equation (49). We are seeking the locus for those (λ,γ) points where the number of real solutions of (49) jumps from one to three. To do this we have to solve

$$f(x,\lambda) = 0, \quad \frac{df}{dx}(x,\lambda) = 0 \tag{53}$$

Explicit elimination of x from (53) produces the desired critical curve

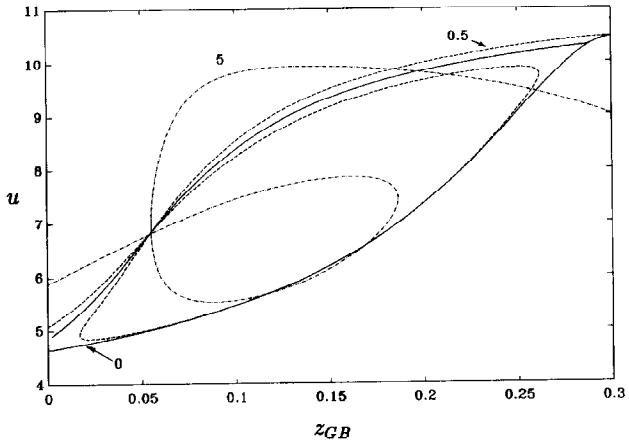

Fig. 20 Surge velocity (ft/sec) versus z_{GB} (ft) for $\delta_s = -20$ (deg) and different values of δ_r (deg)

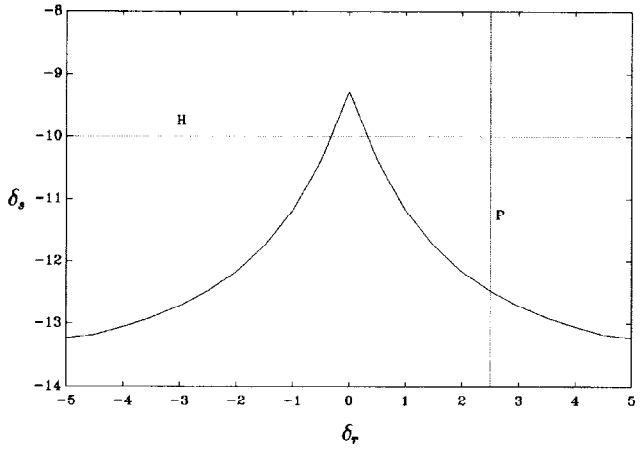

Fig. 21 Cusp singularity in (δ_r,δ_s) parameter plane (deg) and typical paths through cusp

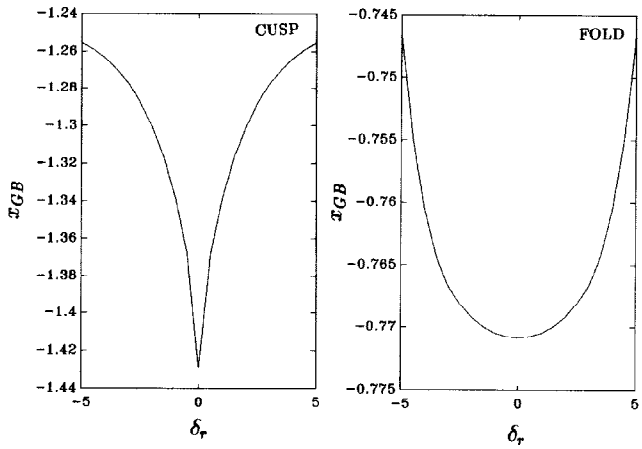

Fig. 22 Cusp and fold singularities in (x_{GB},δ_r) parameter plane (%L,deg) for $\delta_s = -20$ deg

$$4\lambda^3 = 27\gamma^2 \tag{54}$$

which takes the form of a cuspoid with its axis located along the $\gamma = 0$ axis. Under the smooth mappings (50) or (52), the cusp curve (54) maintains its essential characteristics as shown numerically in the following.

The cusp singularity in the (δ_s,δ_r) parameter plane is shown in Fig. 21 for $x_{GB} = -1\%L$, $\delta_B = 2\%W$, and $z_{GB} = 0.1$ ft. This corresponds to the same parameter values used in Figs. 6 through 13. For (δ_s,δ_r) combinations located outside of the cusp, there exists only one steady state, while when crossing the cusp boundary the number of solutions jumps to three. Perpendicular paths through the cusp, i.e., changing δ_s for a given δ_r, produce pitchfork bifurcation diagrams. It can be seen that path P of Fig. 21 generates the corresponding pitchfork diagram of Fig. 6. On the other hand, horizontal paths through the cusp, i.e., changing δ_r for a given δ_s, produce hysteresis bifurcation diagrams as the number of solutions changes from one to three and back to one. A typical example of a hysteresis path is denoted by H in Fig. 21 which generates the solution set seen in Fig. 11.

Similar results can be drawn by considering the bifurcations shown in Figs. 17 and 18. We can see that for $\delta_s = -20$ deg, there exist two distinct pitchfork bifurcations for different values of x_{GB}. These generate two cusp curves in the (x_{GB},δ_r) parameter plane, one of which is shown in Fig. 22. Another point of interest is the turning point shown in Fig. 17 which is located at approximately $x_{GB} = -0.5\%L$ for $\delta_r = 0$. This point is not necessarily associated with any bifurcation phenomena; it simply separates a region where the number of in-plane solutions changes locally from two to zero. In the diagrams shown in Figs. 17 and 18 there exist two turning points, and a typical turning point locus is shown in Fig. 22. It can be seen that, unlike pitchfork points which form cusp singularities, turning points assume the shape of a fold.

Asymmetric cusp curves

As a final prediction tool, we present the biased cusp singularities shown in Fig. 23. These represent the locus of pitchfork points in the (δ_s,δ_r) parameter plane, parametrized by an athwartship location of the center of gravity, y_G, in feet. It can be seen that the axis of the cusp is now located off the $\delta_r = 0$ line. For a given value of δ_r there exists a value of y_G which will produce a symmetric pitchfork bifurcation. Physically, this occurs when the asymmetries associated with each of y_G and δ_r cancel out each other. This pitchfork is of course very degenerate and it immediately changes into perturbed saddle-node diagrams like the ones presented before.

The complete bifurcation surface in the $(\delta_s,\delta_r,\delta_B,x_{GB},z_{GB},y_G)$ parameter space would assume the form of a multidimensional cusp hypersurface. Since direct visualization of this is an impossible task, we can present only slices of the hypersurface as seen on (δ_s,δ_r), (δ_s,x_{GB}), and other two-parameter subspaces. These typical projections appear generically in the form of cusp and fold singularities, as presented above. The actual solution sets can be obtained by lifting the corresponding path through the associated singularity, and they take the various forms of pitchfork sets seen in the previous sections.

Concluding remarks

The problem of steady-state response of submersible vehicles in free positive buoyancy ascent has been studied. Applications of the developed results include ballast control of autonomous underwater vehicles and recovery procedures for submarines under casualty conditions. The main parameters

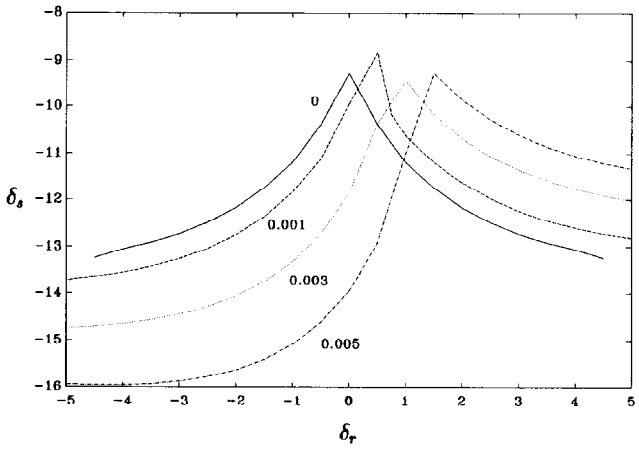

Fig. 23 Biased cusp singularities in the (δ_r,δ_s) parameter plane (deg) and for different values of y_G (ft)

affecting response and stability were the stern plane deflections, amount of excess buoyancy, and the relative positions of the centers of gravity and buoyancy. The main conclusions of this work can be summarized as follows:

1. Motion is not always restricted in the vertical plane even under port/starboard symmetric conditions. Complicated out-of-plane solutions may be generated, and the mechanism for their formation is the pitchfork singularity.
2. A complete characterization of steady-state solutions in the vertical plane was achieved through the organizing center of the winged cusp singularity. Continuation techniques were utilized in conjunction with selected numerical integrations, in order to provide all meaningful solutions in six degrees of freedom.
3. This multidimensional pitchfork unfolds itself in a variety of ways, depending on the particular two-dimensional parameter plane. Such unfolding reported in this work includes pitchfork, separation, hysteresis, teardrops, and terminal, multiple connected, or double pitchforks.
4. Cusp and fold singularities appear in two-parameter design spaces which characterize the number of in-plane and out-of-plane steady-state solutions.
5. An inverted pendulum stabilization due to coupling between an unstable roll mode and stable sway/yaw modes of motion can persist in certain cases, while it can be very degenerate in others.
6. Numerical integrations suggested an extreme sensitivity of the system to initial conditions and parameter values. This sensitivity of solutions was found to occur for parameter ranges which allowed for the inverted pendulum stabilization to occur in the vicinity of a pitchfork bifurcation point.

The primary benefit from such nonlinear dynamics studies is twofold. First, they demonstrate that certain phenomena can be correctly identified and analyzed using rather simplified hydrodynamic modeling. In fact all bifurcation phenomena observed in this work occur at very low angles of attack and drift, and the use of a constant coefficient hydrodynamic model is justified. Second, they can identify regions in parameter spaces where sensitivity of solutions to parameter values and initial conditions is to be expected. It is precisely for these conditions that a more accurate hydrodynamic flow description is needed. The dynamic analysis should then be repeated using the new refined hydrodynamics until convergence. The end product would be a significant enlargement of the vehicle submerged operation envelope as well as the level of confidence for the predicted responses.

Acknowledgments

The authors would like to recognize the financial support of the Naval Postgraduate School Direct Research Fund. Special acknowledgments are due to the primary referee of the paper for his constructive criticism and a number of useful suggestions.

References

AYDIN, I. 1993 Out-of-plane solutions and bifurcations of submarines in free positive buoyancy ascent. Master's thesis, Department of Mechanical Engineering, Naval Postgraduate School, Monterey, Calif.

CLAYTON, B. R. AND BISHOP, R. E. D. 1982 *Mechanics of Marine Vehicles*, Gulf Publishing Co., Houston, Texas.

BOOTH, T. B. 1977 Stability of buoyant underwater vehicles part I. predominantly forward motion. *International Shipbuilding Progress*, **24**, 279.

BOOTH, T. B. 1977 Stability of buoyant underwater vehicles part II. near vertical ascent. *International Shipbuilding Progress*, **24**, 280.

CHEN, H.-C. AND KORPUS, R. A. 1993 A multi-block finite-analytic Reynolds-averaged Navier-Stokes method for 3D incompressible flows. *Journal of Fluids Engineering*.

FALZARANO, J. M., SHAW, S. W., AND TROESCH, A. W. 1992 Application of global methods for analyzing dynamical systems to ship rolling motion and capsizing. *Journal of Bifurcation and Chaos*, **2**, 1.

FALZARANO, J. M. AND ZHANG, F. 1993 Multiple degree of freedom global analysis of transient ship rolling motion. *Nonlinear Dynamics of Marine Vehicles*, The American Society of Mechanical Engineers, ISBN No. 0-7918-1030-5.

GOLUBITSKY, M. AND SCHAEFFER, D. G. 1985 *Singularities and Groups in Bifurcation Theory I*, Springer-Verlag, New York.

GUCKENHEIMER, J. AND HOLMES P. 1983 *Nonlinear Oscillations, Dynamical Systems, and Bifurcations of Vector Fields*. Applied Mathematical Sciences 42, Springer-Verlag, New York.

MCKINLEY, B. D. 1991 Dynamic stability of positively buoyant submersibles: vertical plane solutions. Master's thesis, Department of Mechanical Engineering, Naval Postgraduate School, Monterey, Calif.

PAPOULIAS, F. A. AND MCKINLEY, B. D. 1994 Inverted pendulum stabilization of submarines in free positive buoyancy ascent. JOURNAL OF SHIP RESEARCH, **38**, 1, March, 71–82.

RODDY, R. F. 1990 Investigation of the stability and control characteristics of several configurations of the DARPA SUBOFF model (DTRC model 5470) from captive-model experiments. David Taylor Research Center report DTRC/SHD-1298-08, Bethesda, Md.

SEYDEL, R. 1988 *From Equilibrium to Chaos. Practical Stability and Bifurcation Analysis*, Elsevier, New York.

SMITH, N. S., CRANE, J. W., AND SUMMEY, D. C. 1978 SDV simulator hydrodynamic coefficients, report NCSC-TM231-78, Naval Coastal Systems Center, Panama City, Fla.

THOMPSON, J. M. T., RAINEY, R. C. T., AND SOLIMAN, M. S. 1991 Ship stability criteria based on chaotic transients from incursive fractals. *Philos. Trans. Roy. Soc. London*, **A**, 421.

VIRGIN, L. N. AND BISHOP, S. R. 1988 Complex dynamics and chaotic responses in the Timme domain simulations of a floating structure. *Ocean Engineering*, **15**, 1.